A&A 419, 449–458 (2004)
DOI: 10.1051/0004-6361:20034302
© ESO 2004

Astronomy & Astrophysics

The elliptical galaxy NGC 5044: Stellar population and ionized gas

M. G. Rickes, M. G. Pastoriza, and Ch. Bonatto

Universidade Federal do Rio Grande do Sul (UFRGS), Instituto de Física, Departamento de Astronomia, Brasil
e-mail: [maurogr;mgp]@if.ufrgs.br

Received 10 September 2003 / Accepted 16 February 2004

Abstract. In this work we investigate the stellar population, metallicity distribution and ionized gas in the elliptical galaxy NGC 5044, using long-slit spectroscopy and a stellar population synthesis method. We found differences in the slope of metal-line profiles along the galaxy which suggests an enhancement of α elements, particularly towards the central region. The stellar population synthesis showed that the component with $[Z/Z_{\odot}] \sim 0.0$ dominates the λ5870 Å flux in the central region of NGC 5044, contributing with ∼42% of the total flux, while in the external regions the contribution decreases to ∼8.0%. The component with $[Z/Z_{\odot}] \sim -0.4$ contributes with ∼32% in the central region, and ∼55% in the external regions. The component with $[Z/Z_{\odot}] \sim -1.1$ contributes with ∼26% in the central region, and ∼37% in the external regions. The three components have $\sim 10^{10}$ years. The presence of a non-thermal ionization source, such as a low-luminosity AGN and/or shock ionization, is implied by the large values of the ratio $\frac{[\mathrm{N\,II}]}{\mathrm{H}\alpha}$ observed in all sampled regions. However, the emission lines observed in the external regions indicate the presence of an additional ionization source, probably hot, post-AGB stars.

Key words. galaxies: elliptical and lenticular, cD – galaxies: individual: NGC 5044 – galaxies: fundamental parameters

1. Introduction

A great effort has been made in the last few years to understand how early-type galaxies form and evolve. The relatively recent discoveries that ellipticals are not merely a one-parameter family and that many ellipticals show signatures of interaction with the environment suggest that these galaxies may have different star formation histories, with stellar populations differing in metallicity and/or age (Worthey et al. 1992).

Crucial information on the above issues has been derived from metal line-strength indices (e.g. Davies et al. 1987) and their radial variation inside the galaxies. The Mg2 line-strength distribution in early-type galaxies, for example, can vary considerably, ranging from essentially featureless to structured profiles showing, e.g., changes of slope possibly associated with kinematically decoupled cores, or anomalies in the stellar population of some ellipticals (Carollo et al. 1993b).

NGC 5044 is the central and brightest member of a rich group that contains many dE dwarf members and a few Im and Sm dwarf candidates. The mean radial velocity of the group is ∼2048 km s^{-1} (Ferguson & Sandage 1990). This galaxy presents a very bright ionized gas emission in the form of extended filaments up to 40″ from the center, being larger in the southern part of the galaxy (Macchetto et al. 1996; Goudfrooij 1991). The dust distribution has an irregular morphology, concentrated in the inner 10″, where two central dark clouds can be seen (Ferrari et al. 1999). NGC 5044 has also been detected by IRAS at 60 and 100 μm and also at 6, 12, and 18 μm by ISO (Ferrari et al. 2002). Its IRAS luminosity is $14 \times 10^8\, L_{\odot}$. The galaxy has a nuclear radio source and extended X-ray emission (Fabbiano et al. 1992) and shows a very complex gas and stellar kinematics. The gas velocity profile is very irregular, with many humps and dips; its radial velocity is systematically blueshifted with respect to the stellar systemic velocity by ∼60−100 km s^{-1}. Furthermore, the stellar velocity curves observed on a fairly large area near the galaxy center counter-rotate with respect to the outer regions. Very slow or no stellar rotation is detected along the galaxy's minor axis. The velocity dispersion of the gas peaks at ∼200−230 km s^{-1} in the center, decreasing rapidly outwards (Caon et al. 2000). The peculiar kinematics and gas morphology described above may be signatures either of interactions of NGC 5044 with the environment or a post-merger event.

The goal of this paper is to investigate the stellar population, metallicity distribution and the presence of ionized gas in NGC 5044, which are fundamental parameters to understand the formation and evolution of this galaxy.

This paper is organized as follows: Sect. 2 presents the observations and data reduction; Sect. 3 deals with the equivalent width analysis of the absorption lines and their radial dependence; Sect. 4 describes the stellar population synthesis, whose results are discussed in Sect. 5; Sect. 6 presents an analysis of the emission lines and the nature of the ionization source. Finally, in Sect. 7 a general discussion of the results and conclusions will be drawn.

Send offprint requests to: Ch. Bonatto,
e-mail: charles@if.ufrgs.br

Article published by EDP Sciences and available at http://www.aanda.org or http://dx.doi.org/10.1051/0004-6361:20034302

Table 1. Data obtained at the NASA/IPAC Extragalactic Database (NED) which is operated by the Jet Propulsion Laboratory, California Institute of Technology, under contract with the National Aeronautics and Space Administration.

Parameter	NGC 5044
α(J2000.0)	$13^h15^m23.96^s$
δ(J2000.0)	$-16°23'07.50''$
Morphology	$E0$
M_B	-21.92
B	11.83
$E(B-V)$	0.070
$L_{H\alpha+[NII]}$ (erg s^{-1})	1.28×10^{41}
Radial velocity (km s^{-1})	2704 ± 33
Redshift	0.00902 ± 0.00011
Diameters (arcmin)	3.0×3.0
H_0 (km s^{-1} Mpc^{-1})	75

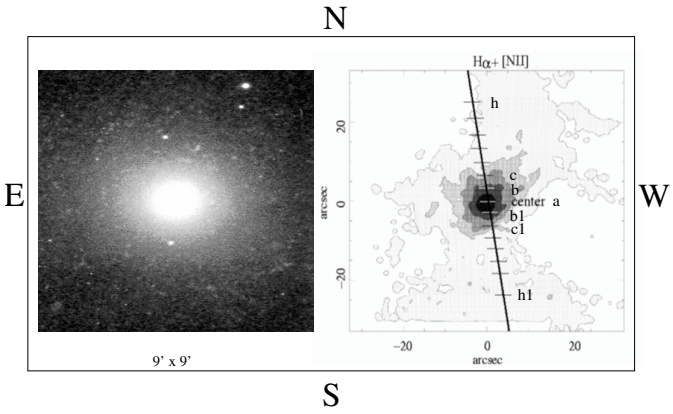

Fig. 1. NGC 5044. *Left panel*: V band image. *Right panel*: slit positioning and spatial extraction on an Hα image. Darker gray corresponds to larger flux.

2. Observations and spectra extraction

NGC 5044 is a bright southern elliptical galaxy for which the general parameters are given in Table 1.

The star formation history, metallicity distribution and emission-gas properties of NGC 5044 are studied using long-slit spectroscopy. The observations were obtained with the ESO 3.6 m telescope at La Silla, Chile, equipped with EFOSC1. The spectra cover the range $\lambda\lambda$5100−6800 Å with a 3.6 Å/pixel resolution. The spatial scale of the observational configuration is $0.6''$ pixel^{-1}; the slit length was $3.1'$ while its width was fixed at $1.5''$ corresponding approximately to the average seeing; two 2-dimensional spectra were obtained with the same exposition time (approximately 45 min) and position angle PA = 10°. The slit positioning on the galaxy is shown in Fig. 1 (right panel), in which the dashes mark the spatial location of each extracted spectrum. A final one-dimensional spectrum was obtained combining (by weighted average) the two extractions for each position marked in Fig. 1.

Details on the extracted spectra are given in Table 2. The spectra have been extracted within different areas in order to increase the signal to noise ratio (S/N), since more external regions have lower flux. Each spectrum was corrected for radial velocity ($V_r = 2704$ km s^{-1}) and Galactic extinction ($A_V = 0.07$). The final average spectra, normalized at λ5870 Å are shown in Fig. 2, separately for the north and south directions on the galaxy.

Table 2. Spatial extractions.

Spectra	R (kpc)	$R/R_{\rm eff}$	Extraction area (kpc)^2
centro	0.00	0	0.06
bN,bS	0.53	11	0.06
cN,cS	1.06	21	0.13
dN,dS	1.59	32	0.19
eN,eS	2.12	43	0.25
fN,fS	2.66	53	0.30
gN,gS	3.19	64	0.30
hN,hS	4.26	85	0.58

Table notes. Column 2: distance of the extraction region to the galaxy center. N and S correspond to the north and south directions, respectively.

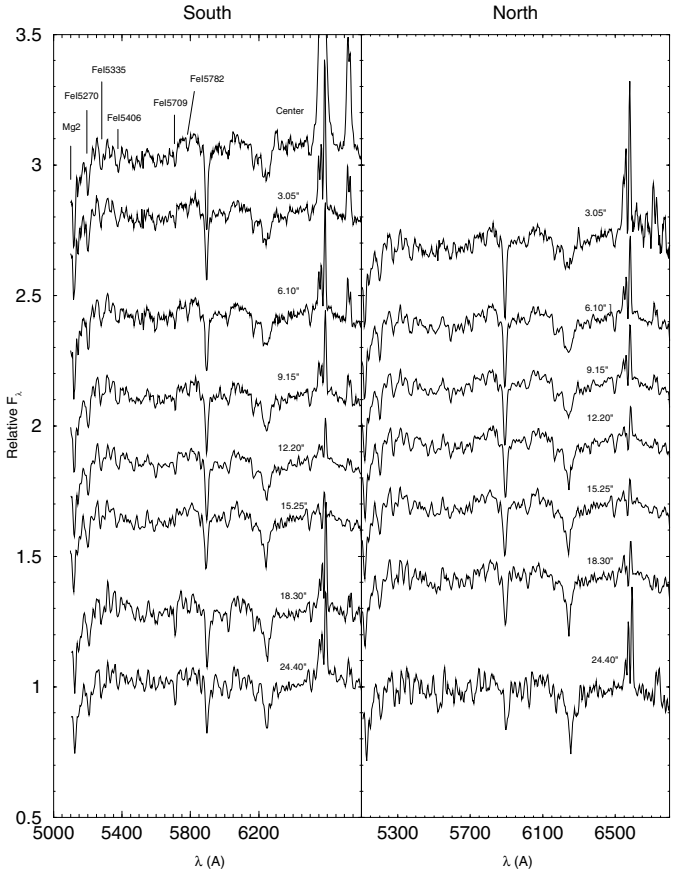

Fig. 2. Spatial extractions for the South (*left panel*) and North (*right panel*) directions normalized at λ5870 Å. The distance to the galaxy center is indicated on each spectrum. Except for the bottom ones, the spectra have been shifted by an arbitrary constant, for clarity purposes.

3. Equivalent width and radial dependence

Elliptical galaxies present systematic variations on the line strength indices Mg2 and Fe I, either from the center to the

Table 3. Lick indices definitions.

Index	Line/Band	$\Delta\lambda$ (Å)	AC (Å)
$Mg2_{Band}$	Mg2	5155.375–5197.875	4896.375–4958.875
			5302.375–5367.375
$Fe_{\lambda 5270}$	Fe I	5247.375–5287.375	5234.875–5249.875
			5287.375–5319.875
$Fe_{\lambda 5335}$	Fe I	5314.125–5354.125	5306.625–5317.875
			5355.375–5365.375
$Fe_{\lambda 5406}$	Fe I	5390.250–5417.750	5379.000–5390.250
			5417.750–5427.750
$Fe_{\lambda 5709}$	Fe I	5698.375–5722.125	5674.625–5698.375
			5724.625–5738.375
$Fe_{\lambda 5782}$	Fe I	5778.375–5798.375	5767.125–5777.125
			5799.625–5813.375

Table notes. Column 3: spectral window; Col. 4: adjacent continuum.

external regions of a given galaxy or limited to the central regions of different galaxies (cf. Gonzáles 1993; Carollo & Danziger 1994a,b; Carollo et al. 1993a; Davies et al. 1993a; Fisher et al. 1995, 1996). Furthermore, the gradients in Mg2 and Fe I have different slopes, suggesting an enhancement of Mg (α elements in general, which are associated with the Super-Novae type I rate) with respect to Fe toward the center of these galaxies. The inferred degree of enhancement seems to increase from dwarfs to massive ellipticals (see Faber et al. 1992; Worthey et al. 1994; Matteucci 1997).

The above arguments suggest the occurrence of changes in some fundamental properties of the constituent stellar population. In order to investigate if NGC 5044, which presents a peculiar stellar kinematics and external ionized gas filaments, has stellar population and metallicity properties similar to those of other elliptical galaxies, we first investigate the spatial distribution of metal-line strengths, and then perform a stellar population analysis.

The present spectra of NGC 5044 cover the spectral range $\lambda\lambda$ 5100–6800 Å which constrains the number of important absorption lines used in stellar population studies. However, in this spectral region the galaxy presents several neutral iron lines, e.g. Fe I$_{\lambda 5270}$, Fe I$_{\lambda 5335}$, Fe I$_{\lambda 5406}$, Fe I$_{\lambda 5709}$ and Fe I$_{\lambda 5782}$, as well as the Mg2 band. These absorption features present strong dependence on the age and metallicity of the underlying stellar population (Bica & Alloin 1986).

Previous to the measurements, all spectra have been normalized at λ5870 Å. The continuum tracing and spectral windows of the absorption lines used in the present paper are those defined by the Lick system (Faber et al. 1985), which are reproduced in Table 3. Each equivalent width (*EW*) and the Mg2 index have been measured three times taking into account the uncertainties in the continuum level definition. This procedure allowed us to estimate the average value and corresponding standard deviation for each measurement.

Although Na I$_{\lambda 5895}$ is the strongest absorption feature present in our spectra, it was not used in the analysis because it may be contaminated by dust concentrated in the central region of the galaxy (Ferrari et al. 1999). Besides the *EW*s and Mg2 index, we measured as well continuum points at 5300 Å, 5313 Å, 5406 Å, 5800 Å, 5870 Å and 6630 Å, as defined in Bica & Alloin (1986). These continuum points, normalized at λ 5870 Å, are listed in Table 5.

In order to compare our results for NGC 5044 with other elliptical galaxies which present similar radial gradients in the Mg2 band and in Fe I$_{5270}$ and Fe I$_{5335}$ lines (e.g. Davies et al. 1987; Carollo et al. 1993a), we first corrected these features for the line broadening due to the internal stellar velocity dispersion.

The spectrum of the G giant star HR 5333 was used to estimate the velocity dispersion correction. HR 5333 was assumed to have zero intrinsic velocity and its spectrum was broadened with a series of Gaussian filters with a velocity dispersion σ varying from 0–300 km s^{-1}, in steps of 10 km s^{-1}.

For each absorption feature considered we calculate an empirical correction index $C(\sigma)$, so that $C(\sigma)_{\rm Mg2} = \frac{\rm Mg2(0)}{\rm Mg2(\sigma)}$, and $C(\sigma)_{\rm FeI} = \frac{W_\lambda(0)}{W_\lambda(\sigma)}$. The velocity dispersion in NGC 5044 varies from ~260 in the center to ~230 km s^{-1} in the external regions (Caon et al. 2000). We have calculated the correction index $C(\sigma)$ for each marked position in Fig. 1 using Caon et al.'s (2000) σ values. Our correction factors vary from 1.23 to 1.27 for the Mg2 index and from 1.20 to 1.23 for the Fe I lines, in the velocity range 230–260 km s^{-1}. Our correction factors for the Mg2 index are somewhat larger than those given by Davies et al. (1993b), while those for Fe I$_{\lambda 5270}$ are similar.

As can be seen in Fig. 3, except for Fe I$_{\lambda 5406}$ (panel (d)), the other absorption features present strong variations with distance to the center. In particular, the Mg2 band (panel (a)) clearly presents a positive gradient, i.e. increasing towards the center of the galaxy, whereas the other Fe I lines present evidence of negative gradients.

3.1. Metallicity gradient

The radial distributions of the Mg2 index and those of the *EW*s of Fe I$_{5270}$, Fe I$_{5335}$, Fe I$_{5406}$, Fe I$_{5709}$ and Fe I$_{5782}$, corrected for velocity dispersion, are shown in Fig. 3. The corrected Mg2 index (panel (a)) presents an enhancement of the gradient which decreases from 0.42 mag in the center to ~0.32 mag in the external regions of the galaxy. On the other hand, the corrected *EW* of Fe I$_{5270}$ (panel (b)) increases from 2.30 Å in the center to ~3.57 Å in the external regions. This result is in reasonable agreement with Carollo et al. (1993a) who found no correlation of the Mg2 index with either Fe I$_{5270}$ and Fe I$_{5335}$. In Fig. 4 we plot the velocity dispersion corrected values of the Mg2 index vs. the *EW*s of Fe I$_{5270}$ and Fe I$_{5335}$, in which we see no correlation between these features. The different slope of the Mg2 gradient relative to those of Fe I$_{5270}$ and Fe I$_{5335}$ can be accounted for by an enhancement of α-elements in general, Mg in particular (Faber et al. 1992; Worthey et al. 1994). In NGC 5044 this effect is more intense in the center than in the outer regions.

The dependence of metallicity gradients on fundamental parameters was investigated by Carollo et al. (1993a) who found that the Mg2 gradient shows a bimodal trend.

Table 4. Mg2 index and *EW*s of the Mg2 and Fe I lines.

	mag	*EW* (Å)					
R ($''$)	$Mg2_{index}$	$Mg2_{band}$	Fe $I_{\lambda 5270}$	Fe $I_{\lambda 5335}$	Fe $I_{\lambda 5406}$	Fe $I_{\lambda 5709}$	Fe $I_{\lambda 5782}$
0	0.416 ± 0.013	13.92 ± 0.51	2.31 ± 0.16	1.14 ± 0.23	0.56 ± 0.01	1.11 ± 0.12	0.89 ± 0.02
3.05S	0.370 ± 0.008	13.33 ± 0.38	2.67 ± 0.11	1.17 ± 0.25	0.96 ± 0.32	1.35 ± 0.03	0.97 ± 0.06
6.10S	0.378 ± 0.001	11.85 ± 0.62	3.11 ± 0.26	1.60 ± 0.50	0.92 ± 0.16	1.46 ± 0.04	1.15 ± 0.20
9.15S	0.339 ± 0.014	11.72 ± 0.70	2.29 ± 0.64	1.21 ± 0.30	0.77 ± 0.24	1.35 ± 0.01	0.93 ± 0.07
12.20S	0.325 ± 0.010	11.20 ± 0.42	3.37 ± 0.01	1.51 ± 0.58	0.96 ± 0.07	1.67 ± 0.24	0.93 ± 0.18
15.25S	0.317 ± 0.014	11.69 ± 0.70	2.87 ± 0.13	1.31 ± 0.30	0.45 ± 0.24	1.45 ± 0.15	0.74 ± 0.23
18.30S	0.364 ± 0.006	11.65 ± 0.51	3.52 ± 0.27	2.57 ± 0.69	0.74 ± 0.22	2.68 ± 0.38	1.41 ± 0.46
24.40S	0.320 ± 0.006	11.23 ± 0.36	3.58 ± 0.62	3.12 ± 0.50	1.22 ± 0.01	2.24 ± 0.26	1.15 ± 0.49
3.05N	0.365 ± 0.017	13.29 ± 0.38	1.99 ± 0.11	2.00 ± 0.25	0.82 ± 0.16	1.08 ± 0.13	0.93 ± 0.13
6.10N	0.364 ± 0.006	12.62 ± 0.62	2.13 ± 0.26	1.67 ± 0.50	0.81 ± 0.07	1.16 ± 0.12	0.85 ± 0.12
9.15N	0.335 ± 0.002	11.47 ± 0.70	1.92 ± 0.12	1.55 ± 0.30	0.63 ± 0.02	0.89 ± 0.12	0.99 ± 0.12
12.20N	0.330 ± 0.007	11.71 ± 0.22	1.93 ± 0.20	1.25 ± 0.58	0.76 ± 0.17	0.78 ± 0.15	0.75 ± 0.15
15.25N	0.330 ± 0.005	11.54 ± 0.17	2.21 ± 0.13	1.16 ± 0.30	0.66 ± 0.20	0.98 ± 0.15	0.64 ± 0.15
18.30N	0.324 ± 0.002	12.33 ± 0.51	2.69 ± 0.27	1.63 ± 0.69	1.37 ± 0.01	1.25 ± 0.01	1.41 ± 0.01
24.40N	0.320 ± 0.010	11.29 ± 0.36	2.92 ± 0.62	1.59 ± 0.50	1.15 ± 0.17	2.05 ± 0.27	0.52 ± 0.27

Table notes. Column 1: distance of the extraction to the galactic center. N and S correspond to the north and south directions, respectively.

Table 5. Continuum points.

	C_λ/C_{5870}					
R ($''$)	λ_{5300}	λ_{5313}	λ_{5546}	λ_{5800}	λ_{5822}	λ_{6630}
0	0.95 ± 0.03	1.02 ± 0.07	0.99 ± 0.02	1.02 ± 0.05	1.02 ± 0.05	0.98 ± 0.12
3.05S	0.99 ± 0.04	1.00 ± 0.01	0.96 ± 0.05	1.00 ± 0.01	1.00 ± 0.02	0.95 ± 0.05
6.10S	1.03 ± 0.05	1.03 ± 0.02	0.98 ± 0.05	1.01 ± 0.02	1.02 ± 0.04	0.95 ± 0.06
9.15S	1.01 ± 0.05	1.02 ± 0.01	0.96 ± 0.06	0.99 ± 0.02	1.00 ± 0.02	0.93 ± 0.05
12.20S	1.01 ± 0.05	1.01 ± 0.01	0.97 ± 0.05	0.99 ± 0.02	0.99 ± 0.01	0.94 ± 0.06
15.25S	1.04 ± 0.05	1.04 ± 0.01	0.98 ± 0.05	1.00 ± 0.01	1.00 ± 0.02	0.92 ± 0.06
18.30S	1.01 ± 0.04	1.02 ± 0.02	0.98 ± 0.04	1.02 ± 0.03	1.01 ± 0.03	0.96 ± 0.07
24.40S	1.02 ± 0.05	1.03 ± 0.02	1.00 ± 0.02	1.01 ± 0.02	1.01 ± 0.02	0.94 ± 0.07
3.05N	0.99 ± 0.06	0.99 ± 0.01	0.95 ± 0.05	0.99 ± 0.01	1.01 ± 0.03	0.95 ± 0.05
6.10N	0.99 ± 0.04	1.00 ± 0.02	0.95 ± 0.06	1.00 ± 0.01	1.01 ± 0.03	0.94 ± 0.05
9.15N	1.00 ± 0.05	1.00 ± 0.02	0.97 ± 0.04	1.00 ± 0.01	0.99 ± 0.02	0.94 ± 0.05
12.20N	1.00 ± 0.04	1.00 ± 0.03	0.97 ± 0.01	0.99 ± 0.03	1.01 ± 0.02	0.95 ± 0.06
15.25N	1.02 ± 0.05	1.02 ± 0.01	0.98 ± 0.05	1.01 ± 0.01	1.01 ± 0.01	0.95 ± 0.06
18.30N	1.00 ± 0.06	1.00 ± 0.02	0.97 ± 0.02	1.00 ± 0.01	1.00 ± 0.02	0.94 ± 0.05
24.40N	1.01 ± 0.05	1.01 ± 0.01	1.01 ± 0.04	1.00 ± 0.01	0.99 ± 0.01	0.93 ± 0.04

Table notes. N and S correspond to north and south respectively.

For objects with masses lower than $10^{11}\,M_\odot$, the Mg2 gradient slope correlates with galaxy mass, whereas for objects more massive than $10^{11}\,M_\odot$, no such correlation appears.

In order to compare our results with the data of Carollo et al. (1993a), first we estimate the mass of NGC 5044 using Poveda's approximation, $M_{\rm tot} = 0.9\,\frac{\sigma^2 R_{\rm e}}{G} = 3.34 \times 10^8\,M_\odot$, where G is the gravitational constant, $R_{\rm e} = 28.53''$ is the effective radius and $\sigma = 256\,{\rm km\,s^{-1}}$ is the central stellar velocity dispersion. According to Fig. 11 of Carollo et al. (1993a), the calculated mass value of NGC 5044 together with the slope of the Mg2 gradient, suggest that this elliptical galaxy was formed by a monolitic collapse.

On the other hand, Kobayashi et al. (1999) have examined line-strength gradients in 80 elliptical galaxies. They found typical gradients $\delta[{\rm Fe/H}]/\delta\log(r) \sim -0.3$, which are flatter than the ones predicted by monolithic collapse simulations. In this paper we found, using the same method, $\delta[{\rm Fe/H}]/\delta\log(r) = -0.31$ which is very close to the value obtained by Kobayashi et al. (1999).

3.2. [Fe/H] abundance

In order to estimate the [Fe/H] abundance in NGC 5044, we use the calibrations Mg2 vs. [Fe/H], Fe I_{5270} vs. [Fe/H] and

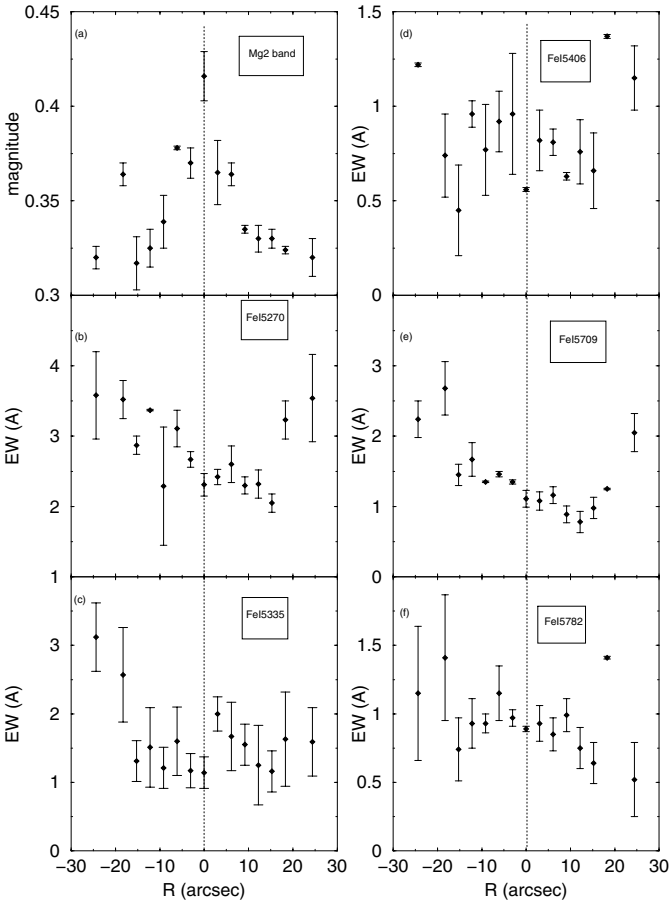

Fig. 3. Spatial variation of absorption features in NGC 5044.

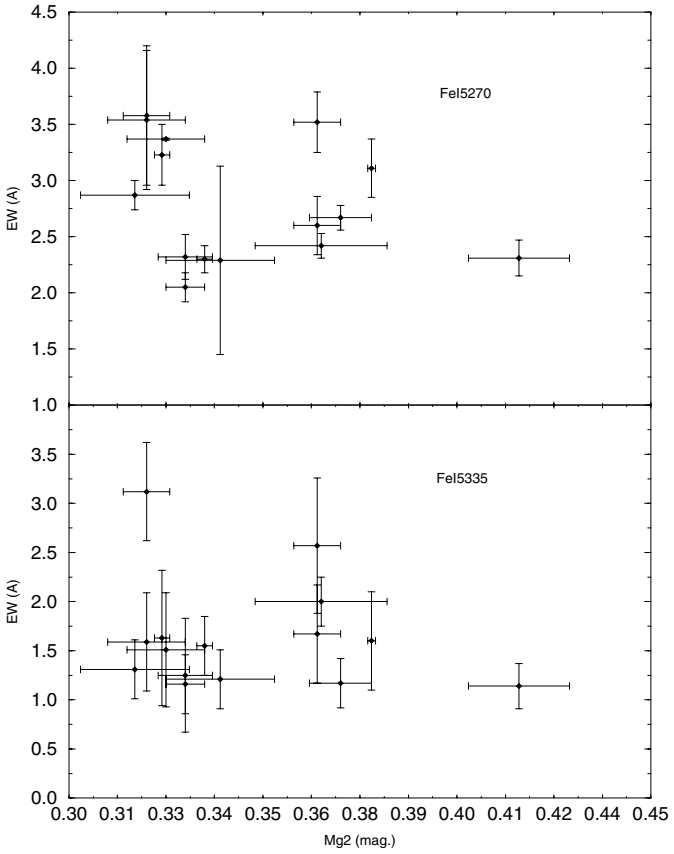

Fig. 4. Mg2 index vs. Fe I_{5270} and Fe I_{5335} line strength.

Fe I_{5335} vs. [Fe/H] presented by Worthey et al. (1992) which are based on models of galactic globular clusters with 18 Gyrs of age. From Fig. 1 of Worthey et al. (1992) we found that for our corrected Mg2 index, [Fe/H] = 0.5 and 0.17 in the central and external regions, respectively. In the same way, using Fe I_{5270} we found [Fe/H] = −0.5, 0.2; and for Fe I_{5335}, we found [Fe/H] = −1.0, −0.5 in the central and external regions, respectively. Therefore, we found an [Fe/H] abundance above solar using as metallicity indicator the Mg2 index, while [Fe/H] is lower than solar for Fe I_{5270} and Fe I_{5335} lines; in addition Mg is above solar in NGC 5044.

4. Stellar population synthesis

For a good understanding of some properties of NGC 5044, such as the presence of central gas emission, a precise determination of the star formation process is necessary. Therefore, the age of the constituent stars in NGC 5044 is an important parameter to be determined.

The integrated spectrum of a given galaxy contains significant information on its stellar content and chemical enrichment (Bica & Alloin 1985). In principle, this information together with a stellar population synthesis method, can be used to determine the star formation history (Bica & Alloin 1986). In this work we employ the stellar population synthesis method developed by Bica (1988) which is based on integrated spectra of star clusters and H II regions, characterized by different ages and metallicities. In the present case, due to the small number of observational constraints (*EW*s and continuum points), we use three old components with different metallicities in order to minimize the degeneracy between age and metallicity of the different population components. These metallicities components (templates) are: $G1 \rightarrow [Z/Z_{\odot}] \sim 0.0$, $G2 \rightarrow [Z/Z_{\odot}] \sim -0.4$ and $G3 \rightarrow [Z/Z_{\odot}] \sim -1.1$, the three with age 10^{10} years.

Alternatively, we have also performed a stellar population synthesis with a set of three components with similar (solar) metallicities and different ages: G1 (10^{10} yr), Y3 (10^{8} yr) and RHII (10^{6} yr). We found that the spectra presented in Fig. 2 are better fitted by a range in metallicities than a range in ages. The base elements that we use are taken from the star cluster population templates described in Bica & Alloin (1986), and are presented in Fig. 5. The corresponding *EW*s and continuum points for the base elements have been measured similarly as those for NGC 5044 and are given in Tables 6 and 7, respectively. We remind that, for the stellar population analysis we use the *EW* of Mg2, which is given in Col. 3 of Table 4.

Basically the algorithm uses the selected *EW*s and pivot points for the continuum measured in a given spectrum and compares them to those of a model computed from a base of simple stellar population elements. The algorithm is not a minimization procedure, instead it generates all combinations of the base elements according to a given flux contribution step. The code also successively dereddens galaxy input continuum points and compares them against a given base model. Every

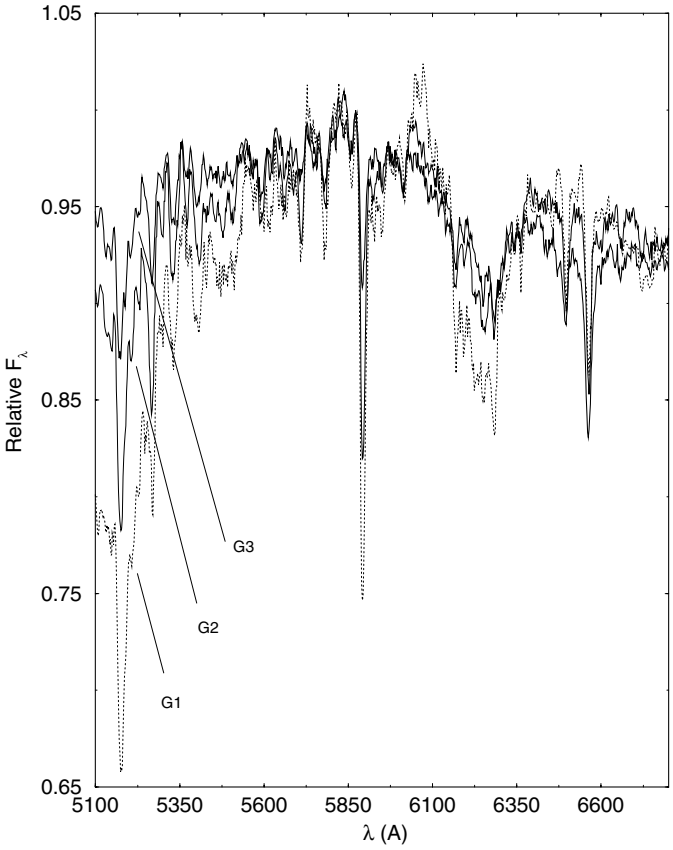

Fig. 5. Population templates (age components) used in the synthesis, normalized at λ5870 Å.

Table 6. Equivalent widths for the base.

	EW (Å)						
	Metallicity $[Z/Z_\odot]$	$Mg2_{band}$	Fe I_{5270}	Fe I_{5335}	Fe I_{5406}	Fe I_{5709}	Fe I_{5782}
G1	∼0.0	5.82	2.77	1.65	1.50	1.36	1.14
Y3	∼−0.4	4.29	2.99	1.70	1.46	1.30	0.80
Y3	∼−1.1	2.75	1.59	0.95	0.77	0.57	0.52

combination is subsequently tested against a set of windows of maximum allowed difference between the observed and the resulting features obtained. Finally, the solutions satisfying all feature windows are averaged out, and this average is adopted as the final synthesis solution.

Initially we used a 10% step for testing flux contribution at λ5870 Å generating about ∼5200 combinations for each assumed $E(B-V)_i$. Reddenings were tested in the range $0.00 \leq E(B-V)_i \leq 0.50$ with a step of 0.01. Thus, in total, ∼260 000 combinations are tested for each extraction, and the number of possible solutions amounts to less than 1%. After probing as above the space of combinations, we calculate the solution with finer steps of 5%, 2% and finally 1%. We tested the Galactic (Seaton 1979), LMC (Fitzpatrick 1986) and SMC (Prévot et al. 1984) reddening laws for the synthesis of each extraction, and concluded that the Galactic law applies in all cases.

Table 7. Continuum points for the base.

	C_λ/C_{5870}					
	λ5300	λ5313	λ5546	λ5800	λ5822	λ6630
G1	0.91	0.97	1.01	1.01	1.00	0.94
G2	0.97	0.98	0.99	1.01	1.00	0.94
G3	0.97	0.99	0.99	0.99	1.00	0.93

5. Synthesis results

The results of our synthesis are given in Table 8, where we present the percentage contribution of each base element to the flux at λ5870 Å. The values of $E(B-V)_i$ are also given in the table.

The G1 component ($[Z/Z_\odot] \sim 0.0$) dominates the λ5870 Å flux in the central extractions of NGC 5044. In the nucleus, the G1 component contributes with ∼42% of the total flux, while in the external regions the contribution decreases to ∼8.0%.

The G2 component ($[Z/Z_\odot] \sim -0.4$) contributes with ∼32% in the central region, and ∼55% in the external regions (24.40″). The G3 component ($[Z/Z_\odot] \sim -1.1$) contributes with ∼26% in the central region, and ∼37% in the external regions, as can be seen in Table 8. Flux fractions and the internal reddening as a function of distance to the center are shown in Fig. 7. Notice that the spatial distribution of the internal reddening $E(B-V)_i$ along the north and south directions (Table 8 and panel (d) in Fig. 7) does not characterize a gradient.

The spectra representing the stellar population of NGC 5044 have been constructed using the star cluster templates (Sect. 4) combined according to the proportions given by the synthesis. We illustrate this procedure in Fig. 6 in which we show the synthesis for the central extraction (top panel). The resulting pure emission spectrum, which is obtained after the subtraction of the population template, is shown in the bottom panel.

The goodness of the above stellar population synthesis method can be assessed by the residuals both in the *EW*s and continuum points. As can be seen in Table 9, most of the absorption features are reasonably well reproduced by the synthesis method. The residuals are almost equally distributed between positive and negative ones, probably indicating that NGC 5044 has the same metallicity than that of the templates. The continuum fit is quite good as well, as can be seen by the residuals in Table 10.

5.1. Integrated colour index

In order to put NGC 5044 in the context of other elliptical galaxies rich in interestellar medium, we build the colour-colour diagram $(J-K)$ vs. $(V-K)$, using the J, K and V photometric data for a sample of elliptical galaxies from Rembold et al. (2002) and NED. The results are presented in Fig. 8, showing that NGC 5044 has the reddest $(V-K)$ colour. This result is probably due to the fact that besides the old stellar population contribution to the $(V-K)$ colour index, NGC 5044 also presents mid-IR (6.7 to 15 μm) dust emission (Ferrari et al. 2002).

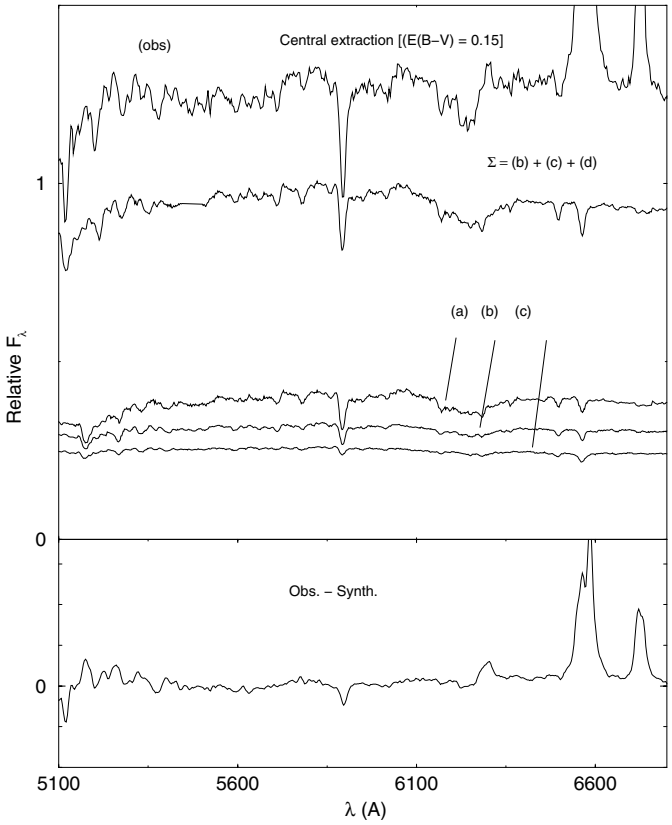

Fig. 6. Stellar population synthesis of the central extraction. *Top panel*: (obs) – observed spectrum corrected for reddening; **a)** – G1 population template; **b)** – G2 population template; **c)** – G3 population template and ($\sum$)-synthesized spectrum. *Bottom panel*: pure emission spectrum. Spectrum (obs) has been shifted by a constant.

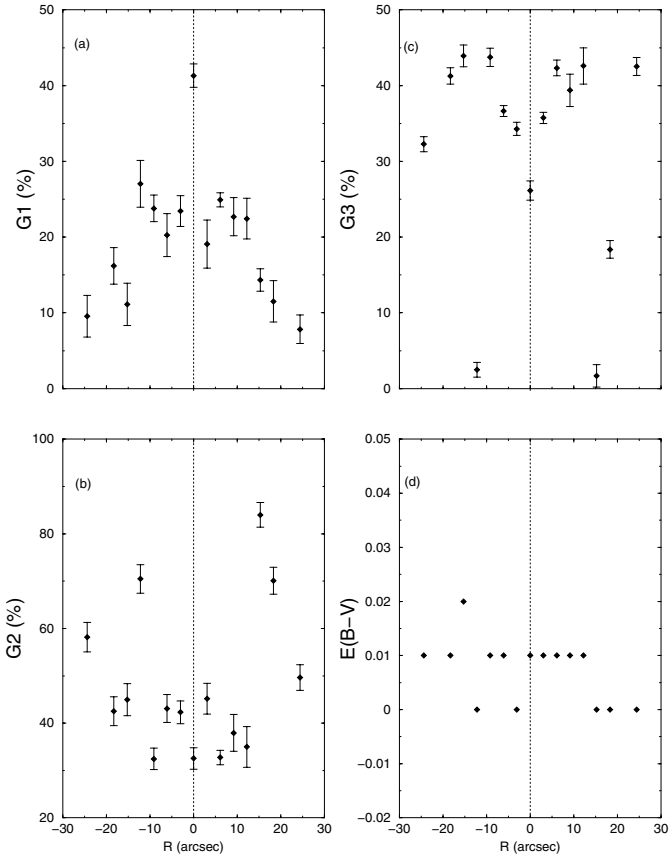

Fig. 7. Synthesis results in flux fractions as a function of distance to the center – panels **a)**, **b)** and **c)**; panel **d)** – spatial distribution of the internal reddening.

Table 8. Synthesis results in terms of flux fractions.

	Flux fraction at λ5870 Å			
R ($''$)	G1 (%)	G2 (%)	G3 (%)	$E(B-V)_i$
0.00	41.31 ± 1.56	32.53 ± 2.30	26.16 ± 1.27	0.01
3.05S	23.43 ± 2.04	42.29 ± 2.40	34.29 ± 0.88	0.00
6.10 S	20.27 ± 2.85	43.09 ± 2.96	36.64 ± 0.73	0.01
9.15 S	23.79 ± 1.76	32.46 ± 2.27	43.75 ± 1.2	0.01
12.20 S	27.04 ± 3.09	70.48 ± 3.01	2.48 ± 0.98	0.00
15.25 S	11.13 ± 2.79	44.95 ± 3.40	43.92 ± 1.45	0.02
18.30 S	16.19 ± 2.42	42.53 ± 3.03	41.28 ± 1.10	0.01
24.40 S	9.57 ± 2.75	58.16 ± 3.14	32.27 ± 1.01	0.01
3.05 N	19.09 ± 3.17	45.17 ± 3.25	35.74 ± 0.74	0.01
6.10 N	24.92 ± 0.95	32.75 ± 1.53	42.33 ± 1.03	0.01
9.15 N	22.69 ± 2.53	37.93 ± 3.89	39.38 ± 2.13	0.01
12.20 N	22.43 ± 2.69	34.97 ± 4.29	42.60 ± 2.40	0.01
15.25 N	14.33 ± 1.49	84.00 ± 2.58	1.67 ± 1.49	0.00
18.30 N	11.52 ± 2.72	70.10 ± 2.84	18.38 ± 1.15	0.00
24.40 N	7.83 ± 1.88	49.64 ± 2.69	42.53 ± 1.20	0.00

Table notes. Column 1: S and N indicate south and north directions, respectively; Col. 5: internal reddening, corresponding to the Galactic law.

Table 9. Equivalent width residuals (Å).

R ($''$)	$Mg2_{band}$	Fe I_{5270}	Fe I_{5335}	Fe I_{5406}	Fe I_{5709}	Fe I_{5782}
0.00	0.48	−0.21	−0.34	−0.73	−0.02	0.02
3.05 S	0.24	0.22	−0.26	−0.27	0.29	0.19
6.10 S	0.85	0.69	0.19	−0.29	0.41	0.38
9.15 S	0.80	−0.02	−0.15	−0.40	0.35	0.17
12.20 S	0.57	0.47	−0.16	−0.49	0.37	0.04
15.25 S	0.94	0.53	−0.05	−0.71	0.46	0.02
18.30 S	0.80	1.16	1.19	−0.44	1.67	0.66
24.40 S	0.32	1.07	1.67	−0.02	1.17	0.41
3.05 N	0.30	−0.45	0.58	−0.40	0.03	0.16
6.10 N	0.67	−0.20	0.30	−0.37	0.15	0.08
9.15 N	0.50	−0.46	0.16	−0.57	−0.14	0.22
12.20 N	0.79	−0.40	−0.12	−0.41	−0.22	0.01
15.25 N	0.08	−0.73	−0.52	−0.79	−0.32	0.20
18.30 N	0.18	−0.01	0.07	0.03	0.08	0.62
24.40 N	0.57	0.55	0.21	−0.02	1.05	0.19

Table notes. Residuals correspond to the observed − synthesized values.

6. Ionized gas

Emission gas has been detected in a large number of elliptical galaxies. However, the origin of this gas and the ionization source are not yet conclusively established. NGC 5044 presents conspicuous emission lines throughout the its body.

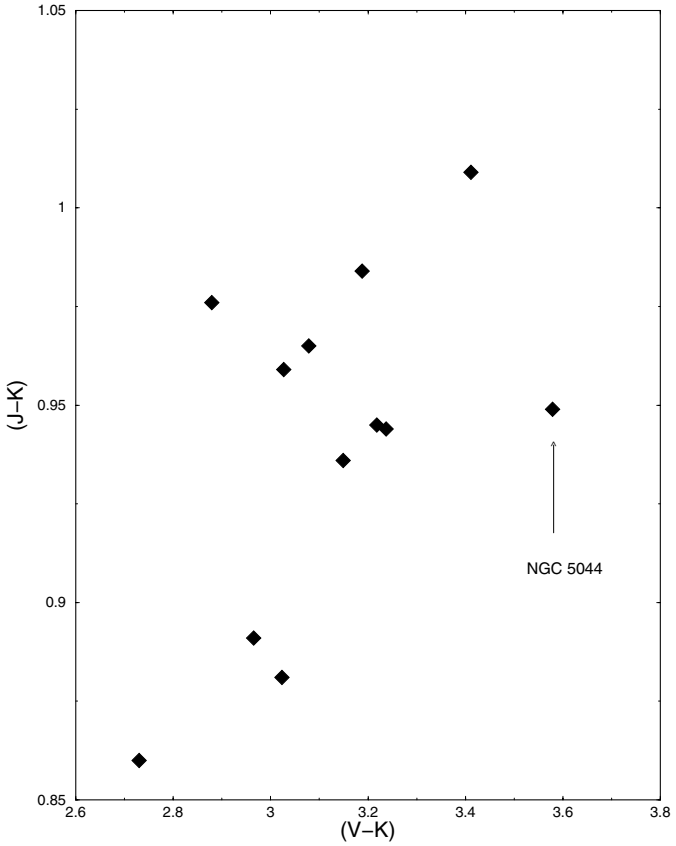

Fig. 8. Colour–colour diagram $(J - K)$ vs. $(V - K)$.

Table 10. Continuum residuals.

R ($''$)	λ5300	λ5313	λ5546	λ5800	λ5822	λ6630
0.00	0.01	0.08	0.01	0.02	0.02	0.04
3.05 S	0.04	0.05	−0.02	0.01	0.00	0.01
6.10 S	0.08	0.08	0.00	0.02	0.02	0.01
9.15 S	0.06	0.07	−0.02	0.00	0.00	−0.01
12.20 S	0.06	0.06	−0.01	−0.01	−0.02	0.00
15.25 S	0.08	0.08	0.02	−0.01	0.00	−0.02
18.30 S	0.06	0.07	0.00	0.03	0.01	0.02
24.40 S	0.06	0.07	0.02	0.02	0.01	0.00
3.05 N	0.04	0.04	−0.03	0.00	0.01	0.01
6.10 N	0.04	0.05	−0.03	0.01	0.01	0.00
9.15 N	0.05	0.05	−0.01	0.01	−0.01	0.00
12.20 N	0.05	0.05	−0.01	0.00	0.01	0.01
15.25 N	0.06	0.06	0.00	0.02	0.00	0.01
18.30 N	0.04	0.04	−0.01	0.01	−0.01	0.00
24.40 N	0.04	0.04	−0.01	0.01	0.00	0.00

Table notes. Residuals correspond to the observed − synthesized values.

The mass of ionized gas in NGC 5044 is estimated between 10^3 and 10^5 $M_\odot$ (Macchetto et al. 1996). In this section we investigate the physical conditions and ionization source of the gas in NGC 5044 using the results of the stellar population synthesis.

The properties of the emission gas are derived from line fluxes, measured in the stellar population subtracted spectra (Sect. 5). The emission lines used in the analysis are: H α, [N II]$_{\lambda 6548}$, [N II]$_{\lambda 6584}$, [S II]$_{\lambda 6717}$ and [S II]$_{\lambda 6731}$. In Table 11 we list, for each extraction region, the absolute flux, the flux

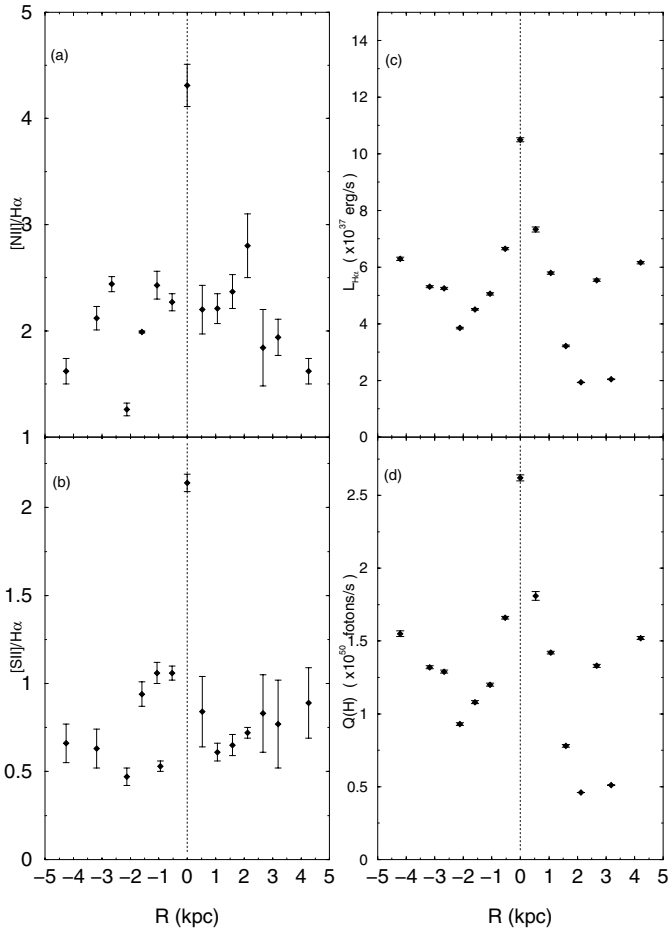

Fig. 9. Spatial distribution of line-ratios and $Q(H)$.

relative to that of H α in the central region, and the *FWHM* for the above emission lines. The uncertainty attributed to each measured flux is based on a gaussian least-squares fit.

Assuming that the emission lines are formed only by recombination, the number of ionizing photons ($Q(H)$) can be calculated as

$$Q(H) = \frac{L_{\mathrm{H}\alpha}}{h\nu_\alpha} \frac{\alpha_B(H^0, T)}{\alpha_{\mathrm{H}\alpha}(H^0, T)}, \quad (1)$$

where the H α luminosity is $L_{\mathrm{H}\alpha} = 4\pi D^2 F_{\mathrm{H}\alpha}$, $\alpha_B(H^0, T)$ is the recombination coefficient summed over all energy levels, and $\alpha_{\mathrm{H}\alpha}(H^0, T)$ is the recombination coefficient at H α. With a Hubble constant of $H_0 = 75\,\mathrm{km\,s^{-1}\,Mpc^{-1}}$, the distance to NGC 5044 is $D = 36$ Mpc. $L_{\mathrm{H}\alpha}$ and $Q(H)$ values are given in Table 12.

In order to infer on the spatial properties of the emission gas, we plot in Fig. 9 the line ratios $\frac{[\mathrm{N\,II}]_{\lambda\lambda 6548,84}}{\mathrm{H}\alpha}$ (panel (a)), $\frac{[\mathrm{S\,II}]_{\lambda\lambda 6717,31}}{\mathrm{H}\alpha}$ (panel (b)), $L_{\mathrm{H}\alpha}$ (panel (c)), and $Q(H)$ (panel (d)).

In the central region, NGC 5044 presents $\frac{[\mathrm{N\,II}]}{\mathrm{H}\alpha} = 4.2$ and $\frac{[\mathrm{S\,II}]}{\mathrm{H}\alpha} > 1$. Notice that the ratio $\frac{[\mathrm{N\,II}]}{\mathrm{H}\alpha}$ is larger than 1.0 for all sampled regions (panel (a)).

In order to investigate the nature of the ionized source in the external regions of NGC 5044, we test two scenarios:

(i) the gas is ionized by an H II region. In order to reproduce the number of ionizing photons observed in the region at 3.05$''$,

Table 11. Emission line parameters.

$R('')$	*lines*	F_λ (10^{-16} erg s^{-1} cm^{-2})	$\frac{F_\lambda}{F_{\mathrm{H}\alpha(\mathrm{R}=0)}}$	*FWHM* (Å)
0.00	Hα	6.80 ± 0.23	1.00	13.62
	[NII]$_{\lambda6548}$	22.0 ± 0.75	3.23 ± 0.15	21.27
	[NII]$_{\lambda6584}$	7.33 ± 0.25	1.07 ± 0.05	21.27
	[SII]$_{\lambda6717}$	8.73 ± 0.16	1.28 ± 0.04	23.64
	[SII]$_{\lambda6731}$	5.83 ± 0.11	0.85 ± 0.03	23.64
3.05S	Hα	4.29 ± 0.11	0.63 ± 0.03	11.82
	[NII]$_{\lambda6548}$	7.34 ± 0.19	1.08 ± 0.04	11.21
	[NII]$_{\lambda6584}$	2.44 ± 0.06	0.35 ± 0.01	11.21
	[SII]$_{\lambda6717}$	2.58 ± 0.08	0.37 ± 0.02	11.10
	[SII]$_{\lambda6731}$	1.96 ± 0.06	0.28 ± 0.01	11.10
6.10S	Hα	3.27 ± 0.14	0.48 ± 0.03	11.78
	[NII]$_{\lambda6548}$	5.91 ± 0.25	0.86 ± 0.04	12.24
	[NII]$_{\lambda6584}$	1.97 ± 0.08	0.28 ± 0.01	12.24
	[SII]$_{\lambda6717}$	2.04 ± 0.10	0.30 ± 0.02	10.73
	[SII]$_{\lambda6731}$	1.42 ± 0.07	0.21 ± 0.01	10.73
9.15S	Hα	2.91 ± 0.11	0.43 ± 0.02	15.08
	[NII]$_{\lambda6548}$	4.36 ± 0.17	0.64 ± 0.03	12.19
	[NII]$_{\lambda6584}$	1.45 ± 0.05	0.21 ± 0.01	12.19
	[SII]$_{\lambda6717}$	1.50 ± 0.08	0.22 ± 0.01	12.12
	[SII]$_{\lambda6731}$	1.24 ± 0.07	0.18 ± 0.01	12.12
12.20S	Hα	2.49 ± 0.09	0.37 ± 0.02	18.32
	[NII]$_{\lambda6548}$	2.36 ± 0.08	0.34 ± 0.01	12.59
	[NII]$_{\lambda6584}$	0.78 ± 0.03	0.11 ± 0.00	12.59
	[SII]$_{\lambda6717}$	0.60 ± 0.05	0.08 ± 0.01	11.12
	[SII]$_{\lambda6731}$	0.57 ± 0.04	0.08 ± 0.00	11.12
15.25S	Hα	3.39 ± 0.20	0.49 ± 0.03	32.46
	[NII]$_{\lambda6548}$	2.41 ± 0.14	0.35 ± 0.02	10.30
	[NII]$_{\lambda6584}$	0.80 ± 0.05	0.11 ± 0.01	10.30
	[SII]$_{\lambda6717}$	0.63 ± 0.03	0.09 ± 0.00	12.84
	[SII]$_{\lambda6731}$	1.15 ± 0.05	0.17 ± 0.01	12.84
18.30S	Hα	3.43 ± 0.13	0.50 ± 0.02	12.55
	[NII]$_{\lambda6548}$	5.47 ± 0.21	0.80 ± 0.04	11.88
	[NII]$_{\lambda6584}$	1.82 ± 0.07	0.26 ± 0.01	11.88
	[SII]$_{\lambda6717}$	1.00 ± 0.15	0.14 ± 0.02	10.26
	[SII]$_{\lambda6731}$	1.15 ± 0.17	0.17 ± 0.02	10.26
24.40S	Hα	4.06 ± 0.23	0.60 ± 0.04	17.73
	[NII]$_{\lambda6548}$	4.88 ± 0.27	0.71 ± 0.05	13.16
	[NII]$_{\lambda6584}$	1.62 ± 0.09	0.24 ± 0.01	13.16
	[SII]$_{\lambda6717}$	1.58 ± 0.21	0.23 ± 0.03	12.98
	[SII]$_{\lambda6731}$	1.09 ± 0.14	0.16 ± 0.02	12.98
3.05N	Hα	4.73 ± 0.38	1.13 ± 0.06	11.08
	[NII]$_{\lambda6548}$	7.84 ± 0.62	1.15 ± 0.10	11.85
	[NII]$_{\lambda6584}$	2.61 ± 0.21	0.38 ± 0.03	11.85
	[SII]$_{\lambda6717}$	2.32 ± 0.45	0.34 ± 0.06	10.73
	[SII]$_{\lambda6731}$	1.63 ± 0.32	0.24 ± 0.05	10.73
6.10N	Hα	3.74 ± 0.14	0.55 ± 0.03	11.08
	[NII]$_{\lambda6548}$	4.56 ± 0.23	0.67 ± 0.04	12.11
	[NII]$_{\lambda6584}$	1.52 ± 0.08	0.22 ± 0.03	12.11
	[SII]$_{\lambda6717}$	0.96 ± 0.07	0.14 ± 0.01	10.61
	[SII]$_{\lambda6731}$	0.70 ± 0.05	0.10 ± 0.01	10.61
9.15N	Hα	2.08 ± 0.11	0.30 ± 0.02	11.32
	[NII]$_{\lambda6548}$	3.51 ± 0.19	0.51 ± 0.03	12.80
	[NII]$_{\lambda6584}$	1.17 ± 0.06	0.17 ± 0.01	12.80
	[SII]$_{\lambda6717}$	0.72 ± 0.06	0.10 ± 0.01	11.35
	[SII]$_{\lambda6731}$	0.63 ± 0.05	0.09 ± 0.00	11.35
12.20N	Hα	1.25 ± 0.10	0.18 ± 0.01	11.74
	[NII]$_{\lambda6548}$	2.65 ± 0.21	0.39 ± 0.03	15.85
	[NII]$_{\lambda6584}$	0.88 ± 0.77	0.13 ± 0.01	15.85
	[SII]$_{\lambda6717}$	0.50 ± 0.02	0.07 ± 0.00	11.00
	[SII]$_{\lambda6731}$	0.40 ± 0.01	0.06 ± 0.00	11.00
15.25N	Hα	3.51 ± 0.17	0.51 ± 0.03	33.26
	[NII]$_{\lambda6548}$	2.41 ± 0.12	0.35 ± 0.02	10.31
	[NII]$_{\lambda6584}$	0.80 ± 0.04	0.12 ± 0.00	10.31
	[SII]$_{\lambda6717}$	0.40 ± 0.09	0.06 ± 0.01	10.89
	[SII]$_{\lambda6731}$	0.37 ± 0.08	0.05 ± 0.01	10.89
18.30N	Hα	1.32 ± 0.09	0.19 ± 0.01	11.45
	[NII]$_{\lambda6548}$	1.93 ± 0.13	0.28 ± 0.02	11.88
	[NII]$_{\lambda6584}$	0.64 ± 9.22	0.09 ± 1.35	11.88
	[SII]$_{\lambda6717}$	0.54 ± 0.14	0.08 ± 0.02	8.76
	[SII]$_{\lambda6731}$	0.48 ± 0.13	0.07 ± 0.02	8.76
24.40N	Hα	3.98 ± 0.22	0.58 ± 0.03	11.66
	[NII]$_{\lambda6548}$	4.82 ± 0.27	0.71 ± 0.05	10.71
	[NII]$_{\lambda6584}$	1.60 ± 0.90	0.23 ± 0.13	10.71
	[SII]$_{\lambda6717}$	1.60 ± 0.13	0.23 ± 0.02	11.87
	[SII]$_{\lambda6731}$	1.95 ± 0.15	0.28 ± 0.02	11.87

Table notes. Column 4: flux normalized to the central region $F_{\mathrm{H}\alpha}$; Col. 5: *FWHM* according to a Gaussian fit.

Table 12. Luminosity and ionizing photons.

$R('')$	$L_{\mathrm{H}\alpha}$ ($\times10^{37}$ erg s^{-1})	$Q(H)$ ($\times10^{50}$ photons s^{-1})
0.00	10.5 ± 0.07	2.62 ± 0.02
3.05S	6.65 ± 0.04	1.66 ± 0.01
6.10S	5.06 ± 0.04	1.20 ± 0.01
9.15S	4.51 ± 0.03	1.08 ± 0.01
12.20S	3.85 ± 0.03	0.93 ± 0.01
15.25S	5.25 ± 0.04	1.29 ± 0.01
18.30S	5.31 ± 0.03	1.32 ± 0.01
24.40S	6.29 ± 0.06	1.55 ± 0.02
3.05N	7.33 ± 0.09	1.81 ± 0.03
6.10N	5.79 ± 0.04	1.42 ± 0.01
9.15N	3.22 ± 0.03	0.78 ± 0.01
12.20N	1.93 ± 0.01	0.46 ± 0.00
15.25N	5.54 ± 0.04	1.33 ± 0.01
18.30N	2.04 ± 0.01	0.51 ± 0.00
24.40N	6.16 ± 0.04	1.52 ± 0.01

Table 13. H II region model.

Spectral type	$\frac{M}{M_\odot}$	Number	$N_{\mathrm{Ly}\,\alpha}$ ($\times10^{48}$ photons s^{-1})
*O*5	30	20	2.00
	22	41	0.25
*B*0	17	75	0.082
	15	101	0.043
	13	142	0.015
	10	264	0.0021

Table notes. Column 3: number of stars of each spectral type.

we have built an H II region according to a Salpeter initial mass function. The H II region model which best reproduces the observed number of ionizing photons is listed in Table 13, where we give the distribution of stars according to spectral type and mass; in the last column we give the number of Ly α photons produced by each star (Dottori 1991). This model H II region produces $\sim2.59 \times 10^{50}$ photons s^{-1} which is comparable to the observed value. However, such an H II region in NGC 5044 would be bright enough to be photometrically detected in visible images obtained with the ESO 3.6 m telescope. The *V*-band image does not present any signature of such an H II region;

(ii) the gas is ionized by a hot, post-AGB star. The number of ionizing photons produced by one post-AGB star with effective temperature of ∼150 000 K corresponds to $\sim6.11 \times 10^{50}$ photons s^{-1}, about 5 times the number of photons observed in the region at 3.05″. The spatial profiles of [N II] and H α extracted along the slit, shown in Fig. 10, reveal that $\frac{[NII]}{\mathrm{H}\alpha} > 2$. However, according to the ionization models for old stars in elliptical galaxies (Binette et al. 1994) the ratio $\frac{\mathrm{N[\,II]}}{\mathrm{H}\,\alpha}$ measured in NGC 5044 could only be produced by a much larger $Q(H)$ than the one we estimate, in particular the high value measured in the central region. Binette et al.'s (1994) models do not reproduce as well the observed ratio $\frac{[\mathrm{SII}]_{6731}}{\mathrm{H}\alpha}$. A high ratio $\frac{\mathrm{N[\,II]}}{\mathrm{H}\,\alpha}$ is characteristic of AGNs.

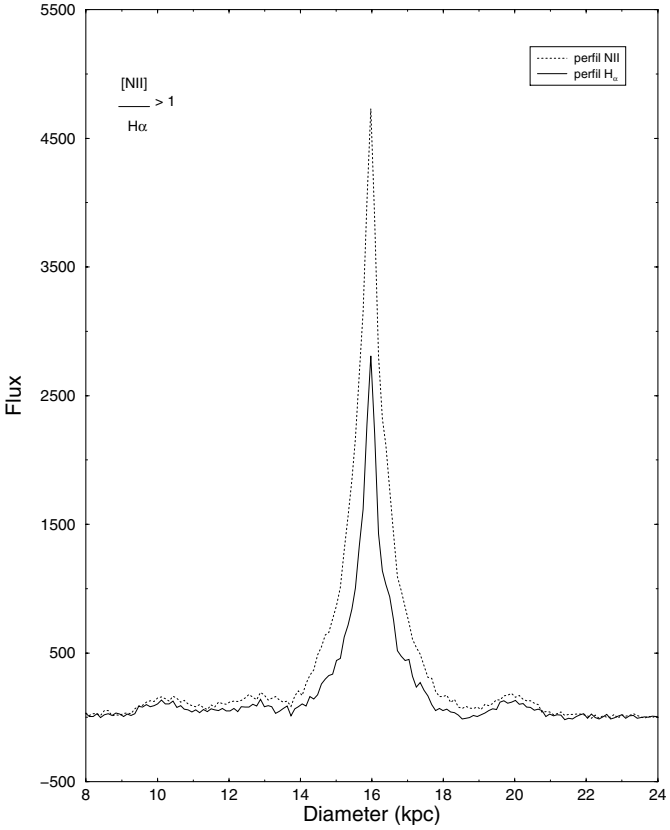

Fig. 10. Spatial profiles of H α and [NII]. Notice that [NII]/H$_\alpha$ > 1 along the galaxy.

In conclusion we find that in the central region the ionization source must be a AGN, while in the external region the lower ratio $\frac{\mathrm{N[II]}}{\mathrm{H}\alpha} \sim 2$ can be accounted for by post-AGB stars.

7. Conclusions

The stellar population, metallicity distribution and ionized gas in NGC 5044 have been investigated in this paper by means of long-slit spectroscopy and stellar population synthesis. With respect to the spatial distribution of metal-strength indices (corrected for velocity dispersion), the Mg2 profile increases towards the central region, contrary to what is observed for the profile of Fe I$_{5270}$. This difference in slopes may be accounted for by an enhancement of α-elements in general, Mg in particular. The Mg2 gradient slope compared with the mass of NGC 5044 indicates a monolitic collapse. However, the measure [Fe/H] gradient slope is not characteristic of one monolitic collapse.

The stellar population synthesis gives that most metallic component ($[Z/Z_\odot] \sim 0.0$) dominates the λ5870 Å flux in the central region of NGC 5044. In the nucleus, this component contributes with ∼42% of the total flux, while in the external regions the contribution decreases to ∼8.0%. The component with $[Z/Z_\odot] \sim -0.4$ contributes with ∼32% in the central region, and ∼55% in the external regions. The metal-poor component ($[Z/Z_\odot] \sim -1.1$) contributes with ∼26% in the central region, and ∼37% in the external regions. The spatial distribution of the internal reddening $E(B-V)_\mathrm{i}$ along the north and south directions does not characterize a gradient.

The large values of the ratio $\frac{\mathrm{[N\,II]}}{\mathrm{H}\alpha}$ observed in all sampled regions characterizes the presence of a non-thermal ionization source, such as a low-luminosity AGN and/or shock ionization. However, in the external regions an additional ionization source is necessary to explain the emission lines, which might be hot, post-AGB stars.

References

Bica, E. 1988, A&A, 195, 79
Bica, E., Arimoto, N., & Alloin, D. 1988, A&A, 202, 8
Caon, N., Macchetto, D., & Pastoriza, M. 2000, ApJS, 127, 39
Carollo, C. M., Danziger, I. J., & Buson, L. 1993a, MNRAS, 265, 553
Carollo, C. M., Danziger, I. J., & Buson, L. 1993b, MNRAS, 553, 580
Carollo, C. M., & Danziger, I. J. 1994a, MNRAS, 270, 523
Carollo, C. M., & Danziger, I. J. 1994b, MNRAS, 270, 743
Davies, R. L., Burstein, D., Dressler, A., et al. 1987, ApJS, 64, 581
Davies, R. L., Sadler, E. M., & Peletier, R. F. 1993a, MNRAS, 262, 650
Davies, R. L., Sadler, E. M., & Peletier, R. F. 1993b, MNRAS, 650, 680
Dottori, H. A. 1981, Ap&SS, 80, 267
Fabbiano, G., Kim, D.-W., & Trinchieri, G. 1992, ApJS, 80, 531
Faber, S. M., Friel, E. D., Burstein, D., & Gaskell, C. M. 1985, ApJS, 57, 711
Faber, S. M., Worthey, G., & Gonzáles, J. J. 1992, in IAU Symp., 149, ed. B. Barbuy, & A. Renzini, 255
Ferguson, H., & Sandage, A. 1990, AJ, 100, 1
Ferrari, F., Pastoriza, M. G., Macchetto, F., & Caon, N. 1999, A&A, 136, 269
Ferrari, F., Pastoriza, M. G., Macchetto, F. D., et al. 2002, A&A, 389, 355
Fitzpatrick, E. L. 1986, AJ, 92, 1068
Fisher, D., Franx, M., & Illingworth, G. 1995, ApJ, 448, 119
Fisher, D., Franx, M., & Illingworth, G. 1996, ApJ, 459, 110
Gonzáles, J. J. 1993, Ph.D. Thesis, Univ. California, Santa Cruz
Goudfrooij, P. 1991, ISSN, 63, 42
Kobayashi, C., & Arimoto, N. 1999, ApJS, 527, 599
Kurucz, R. L. 1979, ApJS, 40, 1
Macchetto, F., Pastoriza, M., Caon, N., et al. 1996, A&A, 120, 463
Matteucci, F. 1997, Fund. Cosmic Phys., 17, 283
Prévot, M. L., Lequeux, J., Maurice, E., Prévot, L., & Rocca-Volmerange, B. 1984, A&A, 132, 389
Rembold, S. B., Pastoriza, M. G., Ducati, J. R., Rubio, M., & Roth, M. 2002, ApJ, 588, 344
Seaton, M. J. 1979, MNRAS, 187, 73
Tantalo, R, Chiosi, C., & Bressan, A., 1998, A&A, 333, 419
Worthey, G. 1994, ApJS, 95, 107
Worthey, G., Faber, S. M., & Gonzáles, J. J. 1992, ApJS, 398, 69
Worthey, G., Faber S. M., Gonzáles, J. J., & Burstein, D. 1994, ApJS, 94, 687